energies

MDPI

Article

Physicochemical Characterization of Phase Change Materials for Industrial Waste Heat Recovery Applications

Angel G. Fernández [1,*], Luis González-Fernández [2], Yaroslav Grosu [2,3] and Jalel Labidi [1]

[1] Department of Chemical and Environmental Engineering, University of the Basque Country, UPV/EHU, 20018 San Sebastián, Spain; jalel.labidi@ehu.eus
[2] Centre for Cooperative Research on Alternative Energies (CIC energiGUNE), Basque Research and Technology Alliance (BRTA), Alava Technology Park, Albert Einstein 48, 01510 Vitoria-Gasteiz, Spain; lgonzalez@cicenergigune.com (L.G.-F.); ygrosu@cicenergigune.com (Y.G.)
[3] Institute of Chemistry, University of Silesia in Katowice, Szkolna 9 Street, 40-006 Katowice, Poland
* Correspondence: angelgabriel.fernandez@ehu.eus

Abstract: The recovery and storage of process heat in industrial applications are some of the key factors to improve the sustainability and reliability of high temperature applications. In this sense, one of the main drawbacks is focused on the selection of proper thermal energy storage (TES) materials. This paper performs a full characterization of four phase change storage materials (PCM), KOH, LiOH, $NaNO_3$ and KNO_3, which are proposed for storage applications between 270 and 500 °C, according to the results obtained through differential scanning calorimeter and thermogravimetric analysis. One of the main innovations includes the corrosive evaluation of these materials in a promising alumina forming alloy (OC4), close to their corresponding phase change temperature during 500 h. The physicochemical properties obtained confirm the optimal use of $NaNO_3$ and KNO_3 and recommend the use, with caution, of KOH, due to its higher corrosive potential. $FeCr_2O_4$, $NiCr_2O_4$ and $FeAl_2O_4$ were the main protective spinels formed in the alloy surface, however, the cross-section study in the alloy immersed in KOH, revealed a non-uniform behavior, presenting some cracks and spallation in the surface. On the other hand, the proposal of LiOH was disregarded since it presents a narrow operation temperature range between melting and solidification point.

Keywords: industrial waste heat; phase change materials; thermal characterization; corrosion

Citation: Fernández, A.G.; González-Fernández, L.; Grosu, Y.; Labidi, J. Physicochemical Characterization of Phase Change Materials for Industrial Waste Heat Recovery Applications. *Energies* **2022**, *15*, 3640. https://doi.org/10.3390/en15103640

Academic Editors: Wenjin Ding, Ziye Ling, Xianglei Liu and Wenji Song

Received: 6 April 2022
Accepted: 13 May 2022
Published: 16 May 2022

1. Introduction

Nowadays, energy is an essential factor to evaluate the economic growth of any country and region as an indicator of its level of development, industrialization and technification, nevertheless, despite the importance of this resource, there are still inefficient behaviors relating to its use, transformation and management, especially at high operation temperatures.

The Industrial sector uses about 37% of the world's total energy and is the largest generator and consumer of process heat from non-renewable sources of energy [1]. Among the objectives set by the European Union for the year 2030, they highlight an important reduction in greenhouse gas emissions (40%), as well as promoting an energy matrix in which 27% of energy must come from renewable sources [1].

In this direction, heating processes are responsible for 17% of energy consumption for industrial purposes and it is wrongly assumed that the heat is incorporated into the products. In fact, a significant part of the heat used in industrial processes (20–50%), as well as that generated in the successive transformations, is dissipated in the form of residual heat, discharged into the environment through the evaporation of water, gases exhaust, coolants, chemical waste, among others [2].

Due to the importance and volumes of these losses, waste heat recovery was recently identified by the International Energy Agency (IEA) as one of the lines to be developed for

the year 2030 [3]. Its recovery is especially interesting, due to its impact on the decrease in economic costs and the growing environmental restrictions imposed on industries, where it is proposed to reduce CO_2 emissions at rates of up to 60% by the year 2040, through better resource management and the implementation of energy efficiency programs [4].

The proposal and integration of TES systems are some of the main important topics of research for industrial process heat recovery. In this direction, the proposal of different thermal energy storage (TES) systems containing PCMs were studied in the literature [5–8]. The main important requirements that an optimal PCM must meet [9] are shown in Table 1:

Table 1. Requirements of phase change materials for thermal energy storage.

Thermophysical	Kinetic	Chemical	Others
-Melting/solidification temperatures in the application range	-*Supercooling* reduced	-Thermal stability/reliability	-Low cost
-High heat capacity			-Low toxicity
-High thermal conductivity	-High crystallization rate	-Low corrosion with the container materials	-Sustainability

As can be seen in Table 1, there are many desirable requirements that phase change materials must meet, but their main selection is based on thermophysical properties, that is, the temperature range where their fusion/solidification occurs, which will correspond to the heat flux to be stored according to the application. H. Mehling and L.F. Cabeza [10] established a classification of PCMs based on their melting point and melting enthalpy (Figure 1).

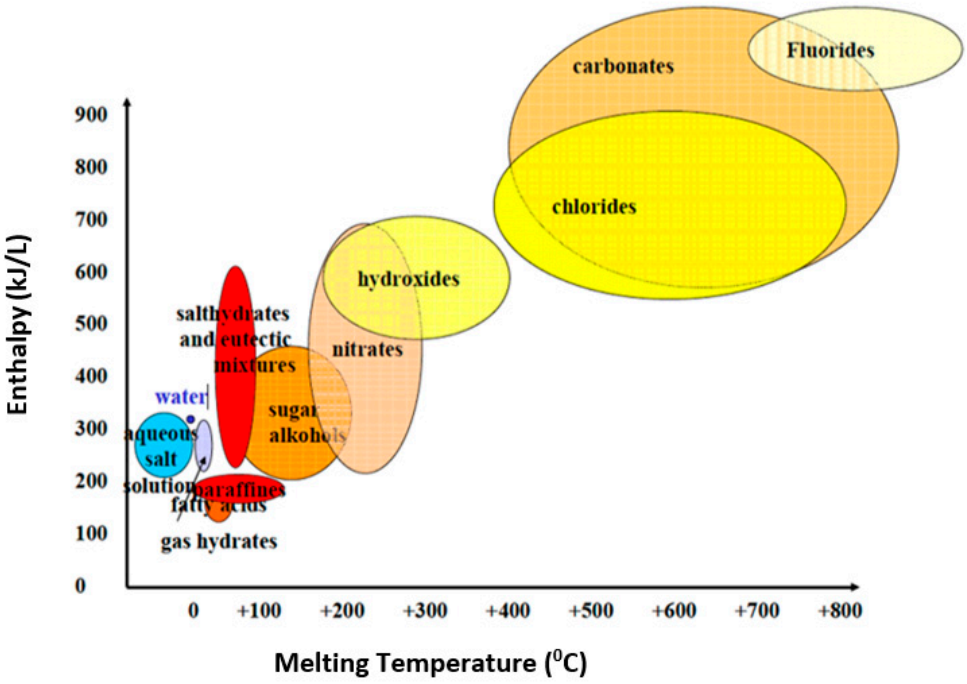

Figure 1. PCMs according to their melting temperatures and enthalpy. Adapted from [10].

Larrinaga et al. [11] established that a higher heat recovery potential could be obtained between 200 and 500°C, especially in the iron and steel sector and the petrochemical industry. This temperature range will be the aim of this paper, nevertheless, few materials' families can act as TES material in this temperature range, where nitrates and hydroxides are the main candidates to be used. Nitrates were widely studied as sensible heat storage materials [12–14] and the main salt proposed is the so-called solar salt, composed of 60%$NaNO_3$ + 40%KNO_3. Moreover, they were widely studied as sensible and latent

heat storage solutions. In this last case, Maldonado et al. [15] proposed this mixture as a PCM material for high temperature power plants, along with myo-inositol ($C_6H_{12}O_6$), developing corrosion tests in different materials at 250 °C during 2000 h and establishing an acceptable corrosion resistance in aluminum and carbon steel. In this direction, the selection of materials for the construction of the salt container presents one of the major challenges to develop feasible TES systems for industrial waste heat recovery applications, and there is a lack of information evaluating the corrosion potential in TES systems able to work between 200 and 500 °C.

The LiOH-KOH mixture was proposed by Cabañas et al. [16] as latent storage media, due to its high energy density and proper melting point for direct steam generation (DSG) technology. The authors [16] carried out a corrosion test of this storage mixture in A516, A316L and in 625, concluding that the lowest corrosion rate (6.3 µm/year) was obtained for A316L. Kuravi et al. [17] provided a list of PCM materials to be used in a high temperature range, but the provided corrosion data refer only to PCMs at a low temperature [18–20], hence more information is required, especially for the corrosive potential, when PCMs for high temperature application are proposed.

The aim of this paper is to carry out a full characterization of the physicochemical properties, including the corrosive potential, of four inorganic phase change material ($NaNO_3$, KNO_3, LiOH and KOH) that could be applied in heat recovery systems between 270 and 470 °C.

2. Materials and Methods

PCMs employed in this research were: KNO_3 (mp: 334 °C, 99.5% purity), LiOH (mp: 462 °C, 99% purity), KOH (mp: 360 °C, 99% purity) and $NaNO_3$ (mp: 308 °C, 99.5% purity), all purchased from Merck (Merck KGaA, Darmstadt, HD, Germany). These materials present an analytical degree; nevertheless, during the experimental work, each salt was handled carefully to avoid water absorption.

Thermal properties as solidification/melting points and fusion enthalpy were analyzed by differential scanning calorimetry (DSC) and the thermal stability was studied by thermogravimetry (TGA). This characterization was carried out in a Simultaneous Thermal Analysis (STA) 449 F3 device from Netzsch, which allows the analysis of all the thermal properties at the same time. A pre-dried sample of each salt was tested in inert atmosphere (nitrogen) for three consecutive heating and cooling cycles between 100 °C and 400 °C for the nitrates, 550 °C for LiOH and 500 °C for KOH. Masses of approx. 70 mg were employed for the measurements and heating/cooling rates of 10 °C/min.

On the other hand, the corrosion studies were carried out using the alumina-forming austenitic (AFA) alloy OC4, an experimental alloy provided by Oak Ridge National Laboratory. The chemical composition of this material is shown in Table 2.

Table 2. Chemical composition of the AFA alloy.

Alloy	Weight %															
	Fe	**C**	**Mn**	**Si**	**P**	**S**	**Cr**	**Ni**	**Cu**	**Ti**	**Al**	**Mo**	**Co**	**V**	**Nb**	**N**
OC4	47.43	0.89	1.80	0.22	0.06	0.01	13.88	26.16	0.57	0.01	4.28	2.24	0.08	0.06	2.27	0.04

Different authors [21–23] have studied the use of alumina-forming alloys, since they can generate alumina scales (generated on the surface of steel) that are more protective than chromia scales, usually formed on conventional stainless steel. OC4 alloy was proposed as a material container in different TES systems using molten salts as nitrates [24] at 550 °C, carbonates [25] at 650 °C and chlorides [26] at 720 °C. The alloy generated a protective alumina scale with high corrosion resistance, especially for nitrate salts, for this reason it was selected to contain the PCM tested in this paper.

The corrosion tests were carried out through an isothermal, static and open to air set-up at 320 °C ($NaNO_3$), 350 °C (KNO_3), 380 °C (KOH) and 470 °C (LiOH), during 500 h.

A scheme of the experimental set up is shown in Figure 2, including the data used for the weight change gravimetric curve.

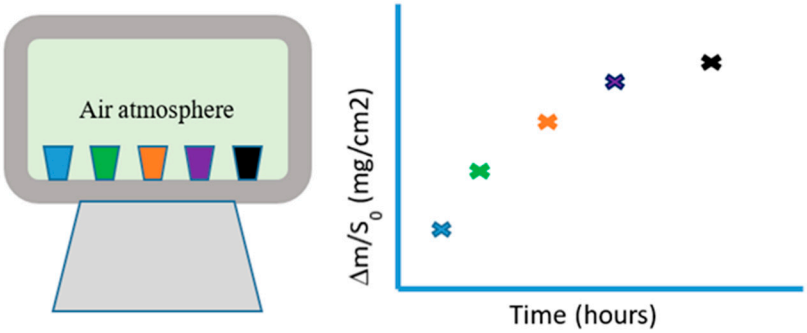

Figure 2. Experimental set up for corrosion tests (**left**) including the data used for the weight change gravimetric curve (**right**).

The coupons used for the isothermal experiment present dimensions of 12 mm × 12 mm × 2 mm, and before the corrosion test they were grounded with #600 SiC abrasive paper, washed with distilled water, degreased with ethanol and dried under a warm air stream, according to the standard procedure of ASTM G1-03 [27]. A digital caliper was used to dimension each coupon before the corrosion test and an analytical balance (with a 0.1 mg responsiveness) was used to weight the coupons introduced in the furnace. The coupons were maintained inside a laboratory desiccator while the molten salt mixture for the corrosion test was prepared. The experimental set up (Figure 2) involved the use of alumina crucibles with the amount of salt mixture recommended by the standard procedure ISO 17245 [28]. The crucibles were introduced inside a resistance furnace and heated through a stepwise heating procedure (maintaining 1 h each heating temperature every 100 °C until the corrosion test temperature). Once the corresponding test temperature was reached, it was maintained for 24 h to homogenize and stabilized the molten salt. Then, one coupon per crucible was introduced to the furnace to start the corrosion test, maintained during 500 h, retrieving the samples after 100, 170, 250, 415 and 500 h. At the end of the exposure time, each coupon was cooled slowly in warm air and cleaned with distilled water to remove the remaining salt. The gravimetric weight change was determined through the Equation (1):

$$\frac{\Delta m}{S_0} = \frac{m_f - m_i}{S_0} \quad (1)$$

where m_i is the original mass of coupons, m_f is the mass of coupons after exposure, and S_0 is the initial area of coupons.

The morphology and elemental composition of the corrosion products were analyzed by Scanning Electron Microscopy (SEM, Quanta 200 FEG model, FEI Company, Hillsboro, OR, USA) coupled to an energy dispersive X-ray spectrometer (EDX). Superficial and cross-section views were examined. For the cross-section, the coupon was imbedded in a resin composed of Aka-Resin and Aka-Cure catalyst (100 g to 12.5 g, respectively). After the complete solidification of the resin, the samples were cut using a precision cutting machine (Struers Miniton) equipped with a diamond blade. Then, the samples were ground by successive SiC sandpapers of increasing grit size up 2500 by means of ATM Saphir stationary polishing machine.

Coupons were also examined by X-ray diffraction (XRD) with a Bruker D8 Discover diffractometer equipped with a LYNXEYE detector using CuKα1 radiation in Bragg–Brentano θ:2θ geometry, to determine the crystallographic phases.

3. Results and Discussion

The study of the thermal properties of the PCM materials selected ($NaNO_3$, KNO_3, LiOH and KOH) were carried out by STA in order to obtain the melting and solidification points, as well as the fusion enthalpy (ΔH_{fus}). The results obtained are shown in Table 3.

Table 3. Thermal properties obtained by STA in $NaNO_3$, KNO_3, KOH and LiOH.

Phase Change Material	Melting Point (°C)	Solidification Point (°C)	Fusion Enthalpy (kJ/kg)	Heat Capacity (J/g K) [29]
$NaNO_3$	299.0	283.5	201.6	1.83
KNO_3	317.5	292.3	92.2	1.48
LiOH	413.1	391.5	Not applicable	3.90
KOH	345.6	336.4	81.6	2.09

The materials proposed as PCMs were also selected based on their heat capacity, in this case, hydroxides presented higher heat capacities compared to nitrate salts [29].

The thermal stability of the molten salts proposed was also tested in Figures 3–5. In this case, a similar behavior was obtained for $NaNO_3$ and KNO_3 (Figure 3), showing a slight initial weight loss due to water content release (0.35%). For the rest of the thermal cycles, the salt weight remained constant during the time between 100 and 400 °C.

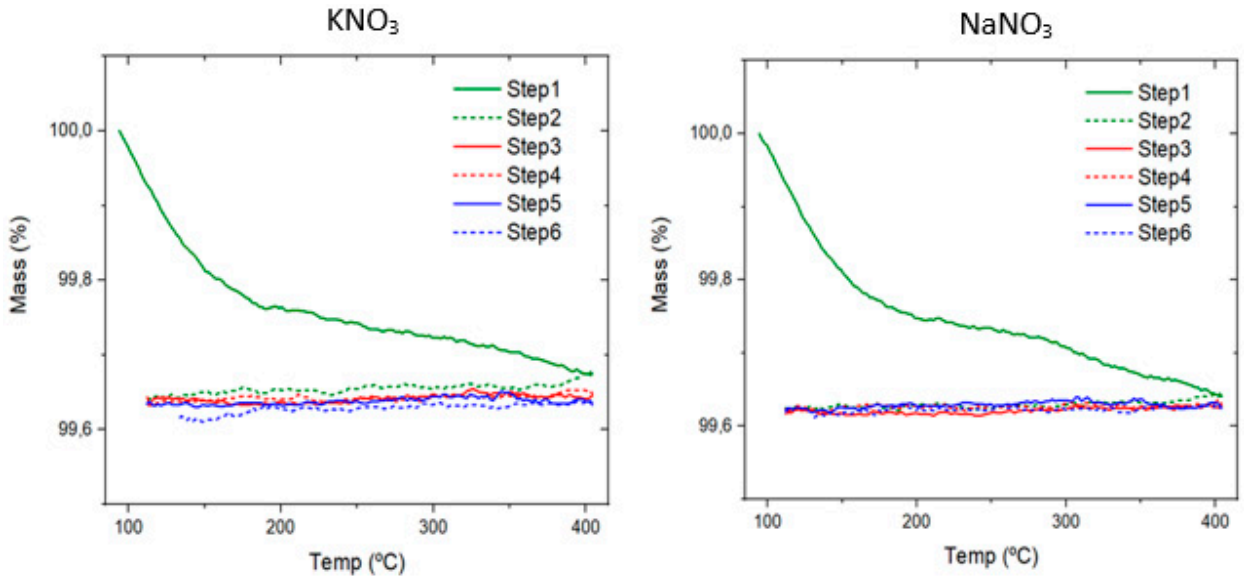

Figure 3. TGA curves for KNO_3 and $NaNO_3$ between 100 and 400 °C.

In the case of KOH, the TGA curve (Figure 4) showed a higher first step compared with the sodium and potassium nitrate. The weight lost due to the water content was 23% in the first cycle of the thermal test, after that, the salt weight remained constant between 100 and 500 °C.

Finally, the TGA curve for LiOH (Figure 5) was carried out from 100 to 550 °C, due to the higher temperature range proposed for the industrial application. In this case, the thermal decomposition has started and it presents a higher increase beyond 500 °C. This is confirmed in the following thermal cycles, where a constant weight loss, around 2% at each thermal segment analyzed, was obtained.

Regarding the corrosion tests performed, four independent studies were carried out for $NaNO_3$ (T = 320 °C), KNO_3 (T = 350 °C), KOH (T = 380 °C) and LiOH (T = 470 °C), during 500 h. The gravimetric curves obtained are shown in Figure 6.

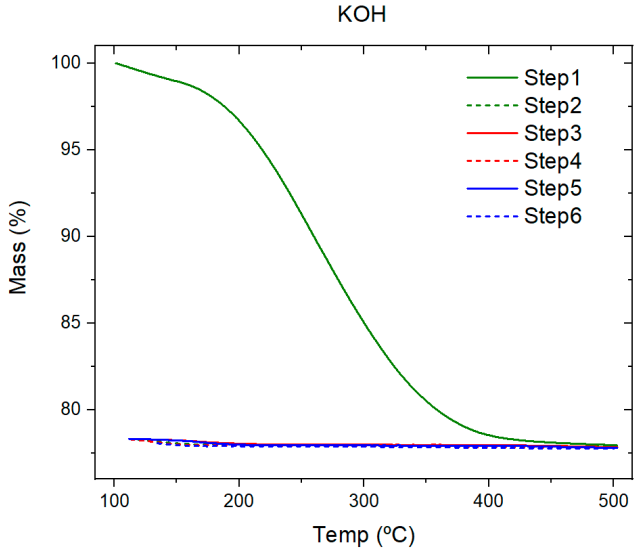

Figure 4. TGA curve for KOH between 100 and 500 °C.

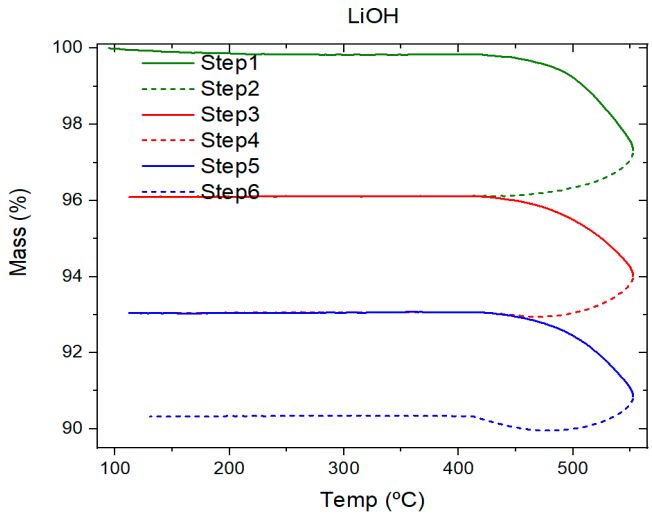

Figure 5. TGA curve for LiOH between 100 and 550 °C.

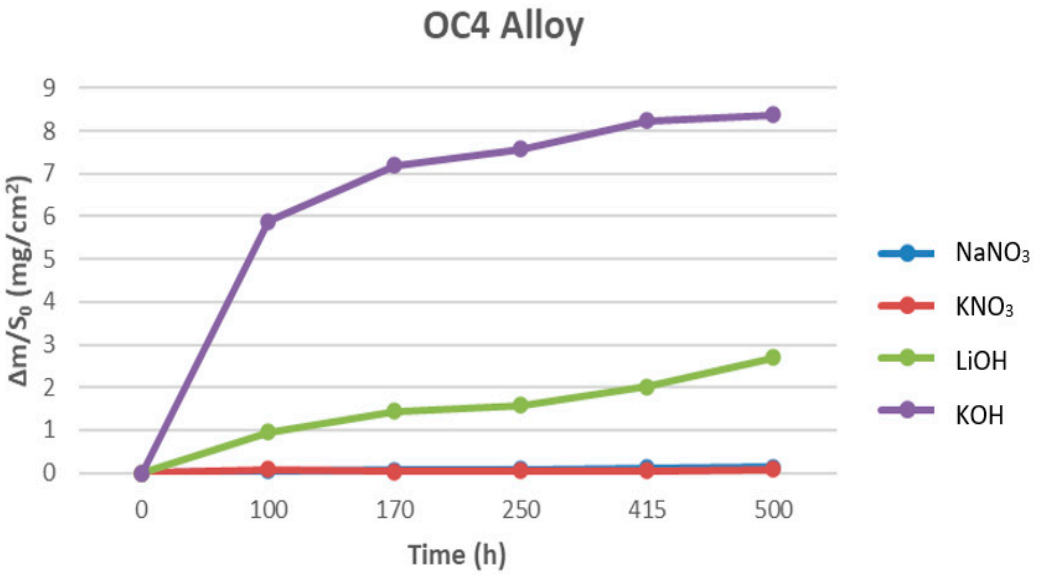

Figure 6. Gravimetric corrosion curves for molten salts tested during 500 h of immersion.

The highest corrosive potential was observed for KOH salt with a mass gain of 8.38 mg/cm^2, which corresponds to a corrosion rate of 0.186 mm/year, follow by LiOH, $NaNO_3$ and KNO_3. It is noteworthy that the lowest corrosive rate was obtained in KNO_3, despite having carried out the test at 350 °C, 30 °C higher than the $NaNO_3$ test.

Scanning electron microscopy studies were carried out for the alloys immersed in lithium and potassium hydroxides, since they presented a higher gravimetric weight change. The superficial image and EDX analysis (at red mark) for OC4 alloy, immersed in LiOH at 470 °C during 500 h, is shown in Figure 7.

Element	*O*	*Al*	*Si*	*Cr*	*Mn*	*Fe*	*Ni*	*Cu*
Weight (%)	7.06	0.44	0.27	7.51	1.86	51.67	23.69	3.08

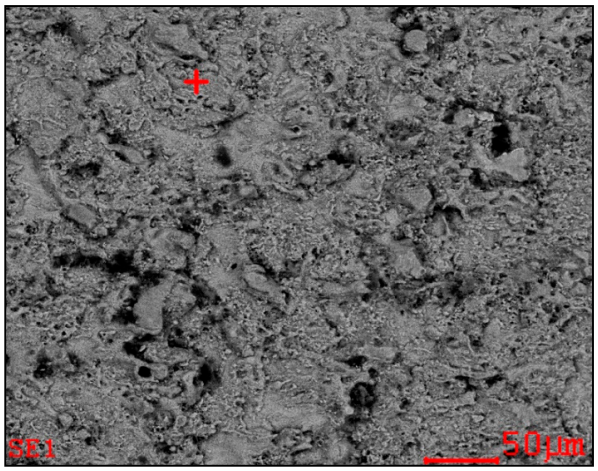

Figure 7. Superficial image of OC4 alloy after 500 h in LiOH at 470 °C.

The study reveals the present of Fe-Cr-O-Ni as main components in the corrosion scale. Some black spots were observed in the alloy and a detailed characterization of this section was analyzed in Figure 8, obtaining a higher content in Al.

Element	*O*	*Al*	*Si*	*Ca*	*Cr*	*Mn*	*Fe*	*Ni*	*Cu*
Weight (%)	27.49	34.64	0.41	2.19	1.92	1.65	19.43	7.99	2.29

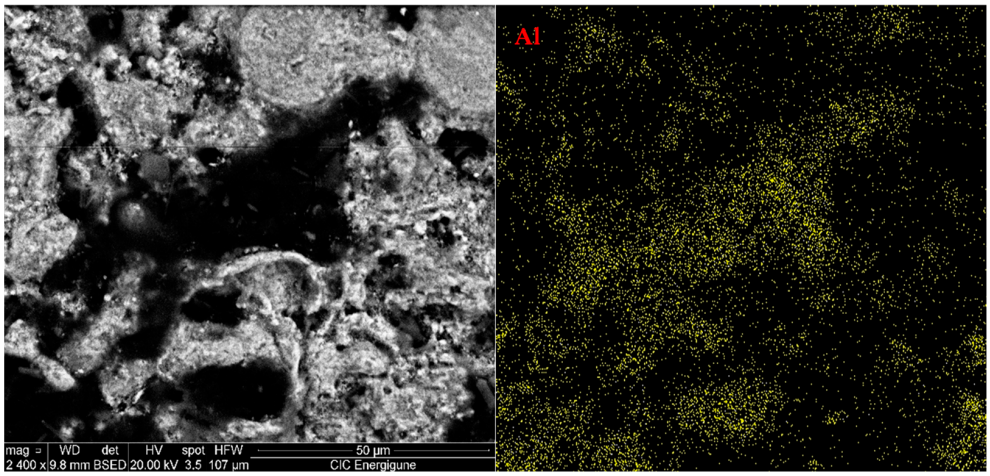

Figure 8. Superficial image magnification of OC4 alloy after 500 h in LiOH at 470 °C and mapping analysis (Al).

This high aluminum content in the surface layer was demonstrated to be a more effective barrier to the attack and penetration of corrosive ions [24–26]. In this case the aluminum content was only detected in these specific black spots, and the protection layer is not uniform. During the corrosion tests, some drawbacks were detected in the proposal of LiOH as PCM, especially related to their high viscosity and the limited operational temperature range, since LiOH starts to decompose as soon as it melts, rendering it necessary to refill the crucible two times during the experimental test. Indeed, some mass loss can be observed at a temperature as low as 420 °C under nitrogen atmosphere (Figure 4), less than 10 °C above the melting point.

On the other hand, the highest corrosion rate was obtained for the OC4 alloy in contact with KOH (Figure 5), despite of the corrosion experiment was carried out at a lower temperature (380 °C) compared the lithium hydroxide salt.

The superficial SEM image (Figure 9) shows several corrosion particles in the alloy surface. A magnification of the corrosion products obtained in the alloy surface is shown in Figure 10.

Element	*O*	*Al*	*Si*	*K*	*Cr*	*Mn*	*Fe*	*Ni*
Weight (%)	5.02	1.36	0.48	3.67	8.40	1.60	50.30	28.63

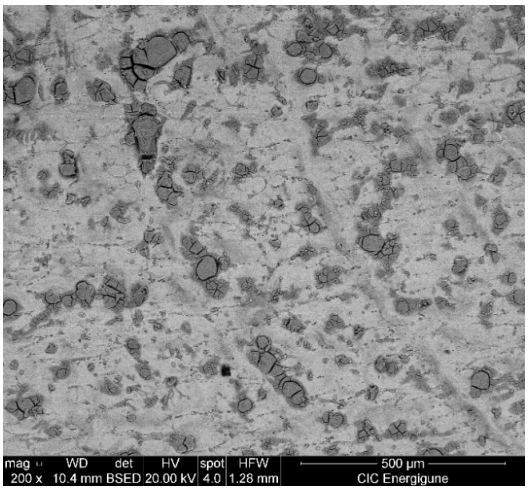

Figure 9. Superficial image of OC4 alloy after 500 h in KOH at 380 °C.

Element	*O*	*Al*	*Si*	*K*	*Cr*	*Mn*	*Fe*	*Ni*
Weight (%)	4.35	0.24	0.26	5.68	1.11	0.68	57.49	29.98

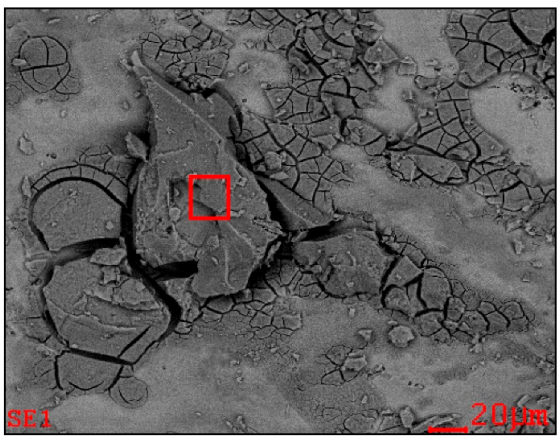

Figure 10. Superficial image magnification of OC4 alloy after 500 h in KOH at 380 °C, including EDX analysis (red square).

The main content of this corrosion product was identified as Fe-Ni-O, including also some potassium content as an impurity from the molten salt. It is worth mentioning that the Cr content is significantly lower in these particles than the average of the corrosion layer (Figure 9).

The formation of this corrosion scale was responsible for the higher weight gain in this salt, showing a non-uniform scale growing. The cross-section study (Figure 11) confirmed this behavior, showing some cracks and spallation in the scale formed.

Element	*O*	*Al*	*Si*	*Cr*	*Mn*	*Fe*	*Ni*
Weight (%) A	8.78	1.18	0.76	1.15	0.56	55.9	31.28
Weight (%) B	-	2.35	0.52	14.82	1.8	52.41	27.27

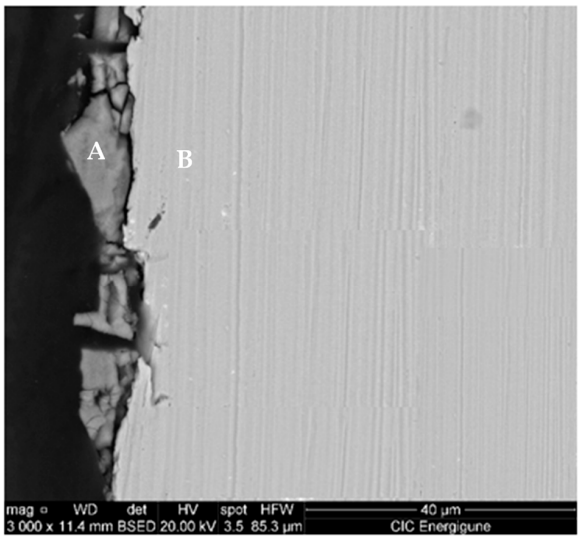

Figure 11. Cross-section image of OC4 alloy after 500 h in KOH at 380 °C, including EDX analysis at A-B point.

The corrosion products formed were identified through XRD, obtained as the main corrosion products $LiFeO_2$, Fe_2O_3 (for LiOH) and NiO and Fe_3O_4 (for KOH). Additionally, some protective spinels with content in aluminum and chromium were detected.

The diffractograms obtained for KOH and LiOH are shown in Figure 12.

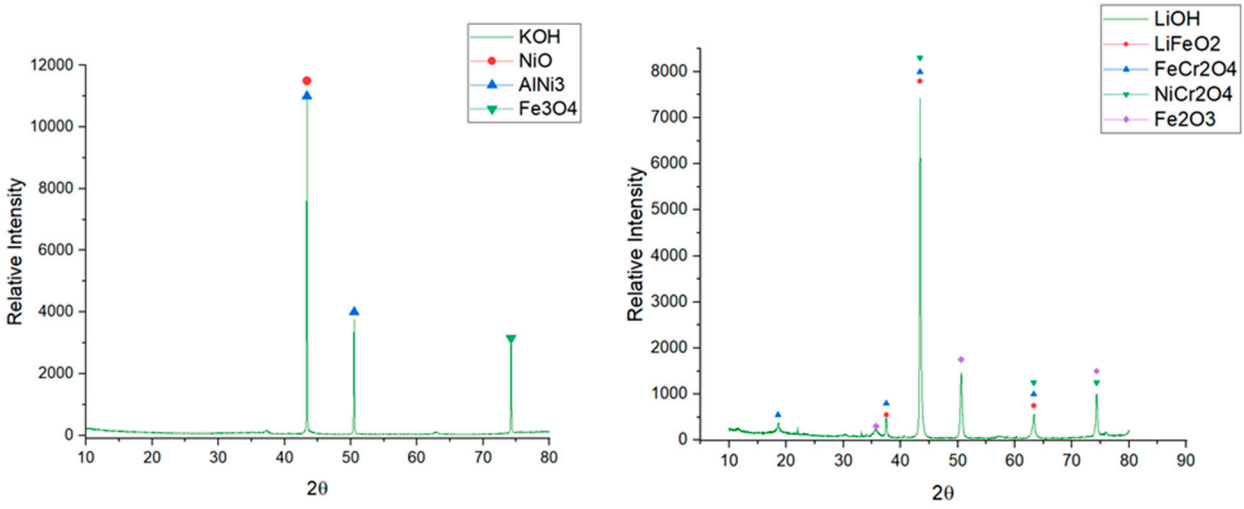

Figure 12. XRD obtained for OC4 alloy immersed in KOH (**left**) and LiOH (**right**) molten salts after 500 h.

The alloy immersed in the LiOH salt presented the formation of $FeCr_2O_4$ and $NiCr_2O_4$ as the main protective components and were responsible for the higher corrosive resistance of this alloy, in comparison with the KOH salt. For KOH, no protective spinels were detected and the OC4 alloy generates NiO and Fe_3O_4 as main oxidation components.

As observed in Figure 11, the corrosion layer formed in OC4 surface showed some cracks and spallation due to the low adherence of the corrosion layer to the alloy. One of these detached layers was analyzed by XRD (Figure 13). It was observed that one of the main protective products formed ($FeAl_2O_4$) was detected in the upper part of the layer formed, presenting a low adherence with the substrate and being easily removed from the alloy surface. In Table 4, a recommendation guide [30] for the levels of corrosion rates in industry is shown. According to this, the OC4 alloy would be recommended for use in contact with LiOH, $NaNO_3$ and KNO_3. In the case of KOH, depending on the application, this recommendation should be managed with caution since the weight gain obtained was 8.38 mg/cm^2.

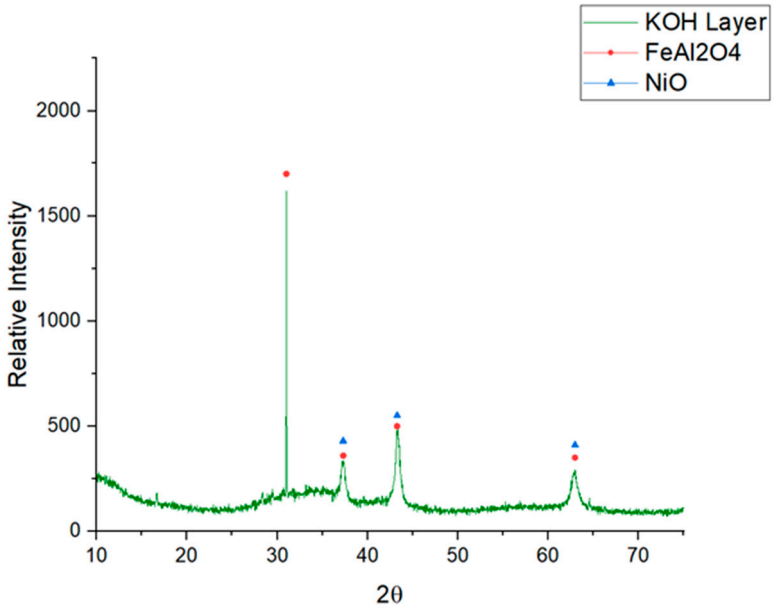

Figure 13. XRD obtained for the layer formed in OC4 alloy immersed in KOH.

Table 4. Recommendation guide for corrosion rates CR in industry. Adapted from Ghali et al. [30].

mg/cm^2 yr.	mm/yr.	Recommendation
>1000	2	Completely destroyed with
100 to 999	0.2–1.99	Not recommended for service (>a month)
50 to 99	0.1–0.19	Not recommended for service (>one year)
10 to 49	0.02–0.09	Caution recommended, based on the specific application
0.3 to 9.9	<0.02	Recommended for long-term service

4. Conclusions

In the last few years, the scientific community working on energy transitions have studied the need for long lasting solutions for improving the performance of industrial processes, especially those that focus on waste heat recovery to increase efficiency in the production and generation of energy. In this direction, the proposal of different storage solutions for high temperature applications were analyzed in the present paper, from 270 to 470 °C. The thermal properties obtained for $NaNO_3$, KNO_3, made them suitable for use between 270 and 500 °C, and obtained an optimal thermal stability after an initial weight loss due to their water content.

KOH also showed a better thermal stability and its use could be extended until 500 °C for use as a PCM for industrial waste heat (IWH) recovery application. On the other hand, LiOH was disregarded since it showed a low operation temperature range between the melting and decomposition point.

Regarding the isothermal corrosion study, the alloy tested (OC4) showed high corrosion resistance, especially in relation to nitrate salts, and it was also proposed as a container material for KOH salts, obtaining a corrosion rate of 0.186 mm/year, due to the formation of protective spinels such as $FeCr_2O_4$ and $NiCr_2O_4$. Longer exposure times, as well as more high-temperature resistant alloys, will be analyzed in future research, due to the promising energy recovery potential involved in the temperature range proposed in this study.

Author Contributions: Conceptualization, A.G.F. and L.G.-F.; methodology, A.G.F. and L.G.-F.; validation, A.G.F. and L.G.-F.; formal analysis, A.G.F.; investigation A.G.F.; resources, A.G.F. and J.L.; data curation A.G.F.; writing—original draft preparation, A.G.F.; writing—review and editing, A.G.F. and L.G.-F.; visualization, A.G.F., L.G.-F., Y.G. and J.L.; supervision, A.G.F., L.G.-F., Y.G. and J.L.; project administration, A.G.F. and J.L.; funding acquisition, A.G.F. and J.L. All authors have read and agreed to the published version of the manuscript.

Funding: This research was funded by [Diputación de Guipúzcoa] grant number [1.0420.200.781.00.04.2021] and Ramon y Cajal program [RyC 2020-28787-I].

Institutional Review Board Statement: Not applicable.

Informed Consent Statement: Not applicable.

Acknowledgments: Angel G. Fernández wants to acknowledge the financial support from Diputación de Guipúzcoa, through the Gipuzkoa Fellows program, and from RyC 2020-28787-I. The authors express their sincere thanks to Cristina Luengo and Yagmur Polat for their technical support.

Conflicts of Interest: The authors declare no conflict of interest.

References

1. Brueckner, S.; Liu, S.; Miro, L.; Radspieler, M.; Cabeza, L.F.; Laevemman, E. Industrial waste heat recovery technologies: An economic analysis of heat transformation technologies. *Appl. Energy* **2015**, *151*, 157–167. [CrossRef]
2. Miró, L.; Brückner, S.; Cabeza, L.F. Mapping and discussing Industrial Waste Heat (IWH) potentials for different countries. *Renew. Sustain. Energy Rev.* **2015**, *51*, 847–855. [CrossRef]
3. International Energy Agency (IEA). Available online: https://www.iea.org/articles/improving-industrial-waste-heat-recovery (accessed on 24 March 2022).
4. Hammond, G.P.; Norman, J.B. Heat recovery opportunities in UK industry. *Appl. Energy* **2014**, *116*, 387–397. [CrossRef]
5. Oró, E.; de Gracia, A.; Castell, A.; Farid, M.M.; Cabeza, L.F. Review on phase change materials (PCMs) for cold thermal energy storage applications. *Appl. Energy* **2012**, *99*, 513–533. [CrossRef]
6. Miro, L.; Gasia, J.; Cabeza, L.F. Thermal energy storage (TES) for industrial waste heat (IWH) recovery: A review. *Appl. Energy* **2016**, *179*, 284–301. [CrossRef]
7. Du, K.; Calautit, J.; Eames, P.; Wu, Y. A state-of-the-art review of the application of phase change materials (PCM) in Mobilized-Thermal Energy Storage (M-TES) for recovering low-temperature industrial waste heat (IWH) for distributed heat supply. *Renew. Energy* **2021**, *168*, 1040–1057. [CrossRef]
8. Nomura, T.; Okinaka, N.; Akiyama, T. Waste heat transportation system, using phase change material (PCM) from steelworks to chemical plant. *Resour. Conserv. Recycl.* **2010**, *54*, 1000–1006. [CrossRef]
9. Nazir, H.; Batool, M.; Bolivar, F.J.; Isaza-Ruiz, M.; Xu, X.; Vignarooban, K.; Phelan, P.; Inamudding; Kannan, A.M. Recent developments in phase change materials for energy storage applications: A review. *Int. J. Heat Mass Transf.* **2019**, *129*, 491–523. [CrossRef]
10. Mehling, H.; Cabeza, L.F. *Heat and Cold Storage with PCM*; Springer: Berlin, Germany, 2008.
11. Larrinaga, P.; Campos-Celador, A.; Legarreta, J.; Diarce, G. Evaluation of the theoretical, technical and economic potential of industrial waste heat recovery in the Basque Country. *J. Clean. Prod.* **2021**, *312*, 127494. [CrossRef]
12. Fernandez, A.G.; Boquera, L.; Cabeza, L.F. Characterization of materials for sensible thermal energy storage at high temperature. In *Recent Advancements in Materials and Systems for Thermal Energy Storage. An Introduction to Experimental Characterization Methods*; Springer: Cham, Switzerland, 2019; pp. 69–88, ISBN 1865-3529.
13. Fernandez, A.G.; Gomez-vidal, J.; Oro, E.; Kruizenga, A.; Sole, A.; Cabeza, L.F. Mainstreaming commercial CSP systems: A technology review. *Renew. Energy* **2019**, *140*, 152–176. [CrossRef]

14. Gil, A.; Medrano, M.; Martorell, I.; Lazaro, A.; Dolado, P.; Zalba, B.; Cabeza, L.F. State of the art on high temperature thermal energy storage for power generation. Part 1: Concepts, materials and modellization. *Renew. Sustain. Energy Rev.* **2010**, *14*, 31–55. [CrossRef]
15. Maldonado, M.; Fernández, A.G.; Cabeza, L.F. Corrosion Assessment of Myo-Inositol Sugar Alcohol as a Phase Change Material in Storage Systems Connected to Fresnel Solar Plants. *Molecules* **2019**, *24*, 1383. [CrossRef] [PubMed]
16. Ruiz-Cabañas, F.J.; Jové, A.; Prieto, C.; Madina, V.; Fernández, A.I.; Cabeza, L.F. Materials selection of steam-phase change material (PCM) heat exchanger for thermal energy storage systems in direct steam generation facilities. *Sol. Energy Mater. Sol. Cells* **2017**, *159*, 526–535. [CrossRef]
17. Kuravi, S.; Trahan, J.; Goswami, D.Y.; Rahman, M.M.; Stefanakos, E.K. Thermal energy storage technologies and systems for concentrating solar power plants. *Prog. Energy Combust. Sci.* **2013**, *39*, 285–319. [CrossRef]
18. Porisini, F.C. Salt hydrates used for latent heat storage: Corrosion of metals and reliability of thermal performance. *Sol. Energy* **1988**, *41*, 193–197. [CrossRef]
19. Cabeza, L.F.; Illa, J.; Roca, J.; Badia, F.; Mehling, H.; Hiebler, S.; Ziegler, F. Immersion corrosion tests on metal-salt hydrate pairs used for latent heat storage in the 32 to 36 °C temperature range. *Werkst. Korros.* **2001**, *52*, 140. [CrossRef]
20. Cabeza, L.F.; Mehling, H.; Hiebler, S. Immersion corrosion tests on metal-salt hydrate pairs used for latent heat storage in the 48 to 58 °C temperature range. *Mater. Corros.* **2002**, *53*, 902–907. [CrossRef]
21. Fernández, A.G.; Rey, A.; Lasanta, M.I.; Mato, S.; Brady, M.P.; Perez, F.J. Corrosion of alumina-forming austenitic steel in molten nitrate salts by gravimetric analysis and impedance spectroscopy. *Mater. Corros.* **2014**, *65*, 267–275. [CrossRef]
22. Yamamoto, Y.; Takyana, M.; Lu, Z.; Liu, C.; Evans, N.; Maziasz, P.; Brady, M.P. Alloying effects on creep and oxidation resistance of austenitic stainless steel alloys employing intermetallic precipitates. *Intermetallics* **2008**, *16*, 453–462. [CrossRef]
23. Brady, M.P.; Magee, J.; Yamamoto, Y.; Helmick, D.; Wang, L. Co-optimization of wrought alumina-forming austenitic stainless steel composition ranges for high-temperature creep and oxidation/corrosion resistance. *Mater. Sci. Eng. A* **2014**, *590*, 101–115. [CrossRef]
24. Fernández, A.G.; Pineda, F.; Fuentealba, E.; Jullian, D.; Mallco, A.; Walczak, M. Compatibility of alumina forming alloys with LiNO3-containing molten salts for solar thermal plants. *J. Energy Storage* **2022**, *48*, 103988. [CrossRef]
25. Fernández, A.G.; Pineda, F.; Walczak, M.; Cabeza, L.F. Corrosion evaluation of alumina-forming alloys in carbonate molten salt for CSP plants. *Renew. Energy* **2019**, *140*, 227–233. [CrossRef]
26. Fernández, A.G.; Cabeza, L.F. Anodic protection assessment using alumina forming alloys in chloride molten salt for CSP plants. *Coatings* **2020**, *10*, 138. [CrossRef]
27. *ASTM G1-03*; Standard Practice for Preparing, Cleaning, and Evaluating Corrosion Test Specimens. ASTM International: West Conshohocken, PA, USA, 2017.
28. *ISO 6892-1*; Metallic Materials—Tensile Testing—Part 1: Method of Test at Room Temperature. International Organization for Standardization: Geneva, Switzerland, 2009.
29. Raznoshinskaia, A.; Troyanovskaya, I.; Kozminykh, V. Heat-storing phase-change materials: Influence of thermophysical properties on stabilization of exhaust temperature. *Mater. Today Proc.* **2019**, *19*, 1831–1834. [CrossRef]
30. Ghali, E.; Vedula, S.; Sastri, E.; Elboujdaini, M. *Corrosion Prevention and Protection: Practical Solutions*; John Wiley & Sons: Hoboken, NJ, USA, 2007; Available online: https://www.wiley.com/en-us/Corrosion+Prevention+and+Protection%3A+Practical+Solutions-p-9780470024027 (accessed on 29 March 2022).